Available online at www.sciencedirect.com
ScienceDirect
ELSEVIER
Ultramicroscopy 107 (2007) 773–780
ultramicroscopy
www.elsevier.com/locate/ultramic

# Exploring the next neighbourhood relationship in amorphous alloys utilizing atom probe tomography

Ahmed Shariq[a,c,*], Talaat Al-Kassab[a], Reiner Kirchheim[a], Ricardo B. Schwarz[b]

[a]*Institute of Material Physics, Georg-August-University, Friedrich-Hund Platz 1, D-37077 Goettingen, Germany*
[b]*Los Alamos National Laboratory, MST Division, Los Alamos, NM 87545, USA*
[c]*Centre of Chemical Engineering & Material Sciences, NUST, B-2, NHS, F11/1, Islamabad, Pakistan*

**Abstract**

A new algorithm is developed to explore the next neighbourhood atomic vicinity from the analysed data obtained using the tomographic atom probe (TAP) technique. The presented algorithm allows to calculate the atomic distances among different next neighbours of different elements as applied to bulk amorphous alloys. The results obtained for $Pd_{55}Cu_{23}P_{22}$ bulk amorphous alloys show reasonable consistency to already available data from different diffraction techniques. The Pd–Pd atoms have highest probability to be a next neighbour than others. The established view that P is not a direct next neighbour to each other is also manifested from these results. Normalizing the distances of the next neighbours to the first neighbour distance in this particular amorphous system possesses a definite order for all elemental correlations. Furthermore, the algorithm was processed for different critical reconstruction parameters to explore the corresponding effect on the distance distribution of next neighbouring atoms. The minor changes in the product of the geometric factor and the evaporation field of the sample does not make any egregious difference on the next neighbourhood evaluation (NNE).


*PACS:* 61.43.Dq; 61.43.Fs; 61.40.+b; 68.37.Vj

*Keywords:* Atom probe field ion microscopy; Data processing; Next neighbourhood evaluation algorithm; Amorphous alloys

## 1. Introduction

The atomic structure is the basis for understanding the nature of all states of matter. Bulk amorphous alloys and metallic glasses are characterized by the absence of atomic long-range order but possess topological and chemical short range ordering with a structural correlation length in the order of atomic distances [1]. The topological structure describes the arrangement of atoms according to the constraint of filling the three-dimensional space, while the chemical structure describes the mutual arrangement of the atoms of different components of the alloy system. Metallic glasses are rapidly quenched liquids produced by avoiding crystallization; whereas bulk amorphous alloys are alloys that can be produced by conventional cooling techniques in bulk dimensions (with a thickness of millimetres rather than micrometers in contrast to metallic glasses). The lack of periodicity in glassy structures encourages scientists to use statistical tools for the description of the structure of amorphous alloys. The structural information of amorphous alloys can best be represented in terms of a radial distribution function (RDF). RDF provides information of average number of atoms at distances between $r$ and $r+dr$ from a given origin atom [2]. These functions are obtained from conventional scattering techniques; using X-rays, electrons or neutrons. For the monoatomic amorphous materials, diffraction provides maximum amount of available structural information. For materials containing $n$ elements, a total of $n(n+1)/2$ distinct pair correlation functions are needed to fully describe the structure. For this reason, different scattering techniques should be incorporated to describe the structure. The combination of different scattering experiments enabled to calculate RDFs and hence, reduced RDFs for simple binary metallic glasses.

*Corresponding author. Tel.: +92 519267660; fax: +92 519267659.
*E-mail address:* ahmed-ccems@nust.edu.pk (A. Shariq).

0304-3991/$ - see front matter © 2007 Published by Elsevier B.V.
doi:10.1016/j.ultramic.2007.02.030

The complex nature of the calculations for multi-component systems makes it even more difficult to elucidate any experimental results, in particular, for the estimation of the partial distribution of the different species in such alloys. Furthermore, RDFs give only spherical averaged information on correlations in atom positions without specifying the unique atom positions and chemical identities of atoms for amorphous materials especially for multi-component systems. Hence, three-dimensional positioning would be required for a complete description. Recently, efforts have been made to address this issue using atom probe field ion microscopy which is proved to be currently the best experimental tool to gain information on chemical heterogeneities at the atomic scale [3–6]. Tomographic atom probe (TAP) data have already been utilized to educe the radial distribution functions [7–9]. In this contribution, an algorithm is presented to extract information about the next neighbourhood atomic vicinity from the TAP data. This algorithm is utilized to specify unique atom positions and chemical identities of atoms for amorphous materials which are difficult to access alone from the RDFs. Using this algorithm, solely TAP experiments divulge all possible correlations for different elements of multi-component systems in real space contrary to the scattering techniques.

## 2. The next neighbourhood evaluation (NNE) algorithm

The NNE algorithm is comparatively similar to the one used for the RDF [7]. Fig. 1 shows a schematic representation of the processing of the NNE algorithm. Atom A with a cross in the centre is chosen as a start atom of a specified volume. Then, the distances and masses from this atom to every other atom in the selected volume are calculated. The neighbouring limit can be chosen to be 1000 or 1500 atoms. These distances are then listed in the ascending order, along with the chemical nature to that of the start atom. Similarly, the next atom is then selected as a start atom (atom B in the centre of the dot-dashed circles in Fig. 1) and the same procedure is repeated until the whole selected volume is processed. The distances and chemical nature of the neighbours of all atoms are then summarized in a table containing information of the first 1000 or 1500 neighbours of each atom. The experimental histogram of any neighbour can be then drawn. The distance for the maximum of such histogram gives us the maximum probability of finding an atom.

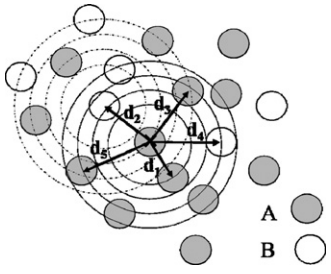


Fig. 1. Schematic sketch illustrating the basic consideration for the next neighbourhood evaluation algorithm. Atom A, having a cross in the centre is chosen as a first atom in the presented volume. The distances and chemical nature of the next neighbouring atoms are calculated in ascending order, until the pre-selected next neighbouring limit is reached. Then next atom is selected as a start atom, in this case B atom in the centre of the dot-dashed line circles and the same procedure is repeated until the whole selected volume is processed.

## 3. Experimental details

The NNE algorithm is applied to Pd-based bulk amorphous alloys for elucidating the atomic distance between neighbouring atoms. The $Pd_{55}Cu_{23}P_{22}$ bulk amorphous alloys were produced as a 2 mm diameter rod with the length of almost 50 mm at Los Alamos National Laboratory, Los Alamos, USA. These rods were later cut into 2 mm diameter discs with a thickness of 1 mm using an electric discharge machine (EDM) for the differential scanning calorimetry (DSC) measurements. DSC was carried out by using Perkin-Elmer Pyris DSC 7 with a heating rate of 0.33 K/s.

With the EDM, TAP samples were cut into $0.3 \times 0.3 \times 10\,mm^3$ rods from the bulk samples. Needle-like specimens of as cast sample were prepared by two step electropolishing for TAP analysis. Twenty-five per cent perchloric acid in glacial acetic acid, floating on trichloroethylene was used for the first step while final thinning was done in 2% perchloric acid in ethyleneglycol–monobutylether. One of the challenges in successful TAP analysis is having a very sharp specimen free of surface contaminations that might induce brittleness. This becomes even more critical in the case of bulk metallic glasses which are well-known for their brittle nature. The conventional electropolishing method may leave a complex oxide layer enveloping the outer surface of the tip making it even more brittle [10]. The tip of the needle-like specimen was cleaned with a focused ion beam using annular gallium ions [11]. The FEI Nova$^{TM}$ 600 Nanolab dual beam (FIB/SEM) instrument was used for ion milling. The 3-DAP investigations were performed with a TAP detector [12,13]. During TAP analysis, a pulse fraction of 20% between the pulse voltage and the permanently applied voltage was used with a pulse repetition rate of 2000 Hz. TAP analyses were performed at a temperature of 30 K to have the least thermal influence during field evaporation.

## 4. Experimental results

The DSC traces for the investigated $Pd_{55}Cu_{23}P_{22}$ amorphous alloy reveal a glass transition at 263 °C, the start of crystallization around 317 °C and a pronounced crystallization peak at 332 °C. A homogeneous random atomic distribution is shown by the three-dimensional atomic reconstruction of the as cast sample in Fig. 2. A comparison of the frequency distribution of the experimental data and that from a binomial distribution with the same mean concentration for each constituent

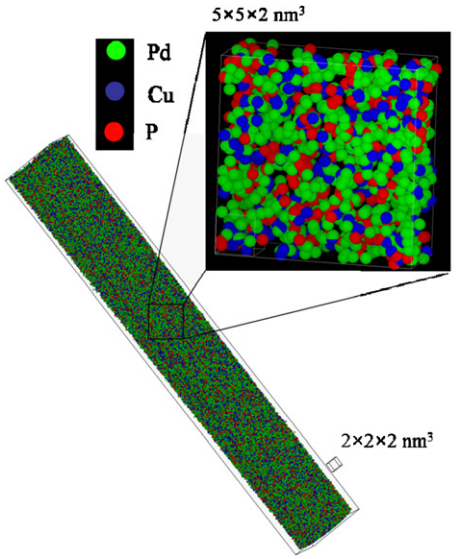


Fig. 2. Three-dimensional atomic reconstruction for $Pd_{55}Cu_{23}P_{22}$ bulk amorphous alloy.

Table 1
Summary of the calculated $\chi^2$ values for the $Pd_{55}Cu_{23}P_{22}$ bulk amorphous alloy

| | Pd | Cu | P |
|---|---|---|---|
| $\chi^2$ | 27.7 | 27.1 | 35.7 |
| $\chi^2$ alpha | 43.8 | 37.6 | 37.6 |
| Degree of freedom | 30 | 25 | 25 |

The value of $\chi^2$ alpha is also given for comparison, with the significance level of alpha i.e., 0.05.

reveals no palpable deviation from a random solid solution. The $\chi^2$ values calculated are summarized in Table 1. Miller has reported nanometre scale copper-enriched/phosphorous-depleted regions and vice versa in Pd–Cu–P bulk amorphous alloys with different compositions [14]. However, our studies reveal a homogeneous distribution, the plausible explanation for the diverse results are different thermal histories (cooling rate during sample preparation) in addition to the differences in composition of the investigated materials.

The NNE algorithm is processed for a $10 \times 10 \times 10\,\mathrm{nm}^3$ volume chosen from the centre of the analysed volume. Albeit, the gallium ion damage to the specimen during the ion milling is limited to first 10–20 nm, the selection of a volume from the centre ensures that the irradiation damage do not effect the local chemical order. Selecting only Cu–Cu elemental correlation in the analysed volume, the experimental histograms are drawn for the first five neighbours as shown in Fig. 3 (only first five neighbours are chosen for simplicity). The distributions of the distances of the next neighbouring atoms in the histograms are denoted as NN*i*. The occurrence of the distances for all neighbours follows a Gaussian distribution. This distribution provides the information about the probability of finding first five neighbouring Cu atoms at certain distances. This figure also reflects the experimental errors in positioning where the peaks are broadened considerably in comparison to the expected ideal peak distribution. Since the inter-atomic distances in a given reconstructed volume may as well depend on the detection efficiency, a slight shift in the position of the peak would also occur as a consequence.

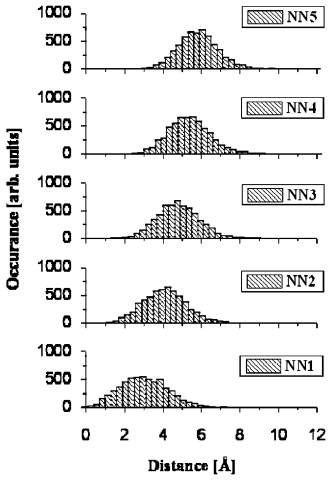


Fig. 3. Histogram showing the distance distribution of first five next neighbours for Cu–Cu correlation.

If $P(r)$ is a true distribution of the first next neighbour distance and $P^o(r)$ is its apparent distribution due to the experimental broadening, then the relation can be described mathematically as

$$p^o(r) = \int \mathrm{d}^3\overline{r'} s(\bar{r} - \overline{r'}) p(r'),$$

where $s(\bar{r} - \overline{r'})$ represents the experimental broadening of the atomic distribution. As a matter of fact, two atoms cannot occupy a position less than their average diameter, the distribution of the first neighbour should start from a critical distance $r_c$ rather than from 0 as shown in Fig. 4 for the first next neighbour (NN1). Another important parameter is the value of the full-width at half-maximum (FWHM). The experimental broadening, $s(\bar{r} - \overline{r'})$ leads to a higher value of the FWHM than reality. One of the major factors leading to the experimental broadening is detection efficiency (i.e., 50%). Higher detection efficiency will result in higher number of atoms in total, to which the averaged NNs will be more precise, as represented by the ideal distribution in Fig. 4. Nevertheless, the peak positions in these distribution plots give important information about the distances of the next neighbours.

The Gaussian fit for all histograms gives the probability of finding first five neighbouring Cu atoms at certain distances as shown in Fig. 5. This figure is a reproduction of Fig. 3, after a Gaussian fit, however, also includes the subsequent Gaussian fits to other correlations. The maximum of Cu–Cu next neighbour atomic distribution

peaks gives us the maximum probability of finding relative Cu atoms which is same as the average of all the distances of the first neighbouring atoms. Similarly, Fig. 5 also shows the distribution of the next neighbouring atoms for other elemental correlations calculated by processing this algorithm. All other correlations follow a likewise trends as that of the Cu–Cu correlation, shown in Fig. 3. The FWHM for each correlation shows the following trend.

FWHM for NN1 > NN2 > NN3 > NN4 > NN5.

This relation reveals that the distribution for NN5 has the smallest error among all of them. The experimental limitations in TAP analysis (i.e., detection efficiency, depth and lateral resolution, localised effect of field evaporation, etc.) result in smearing individual next neighbouring atomic distributions leading to strong overlapping (see Fig. 5). This comparison also provides plausible explanation of inability to reveal any detailed structure in the RDFs [7,15] due to the pronounced overlaps in NN's atomic distributions. Albeit, there is no problem in differentiating individual NN distributions which is evident from Fig. 3 (experimental histograms), the smearing effect however pose greater uncertainty in differentiating coordination shells in the RDFs [15]. A comparison of FWHM among different correlations reveals following trend: Pd–Pd < Cu–Cu < P–P, that depends on the respective concentration of different species in the analysed volume. Averaging over larger number of atoms of a certain element (i.e., higher concentration) will

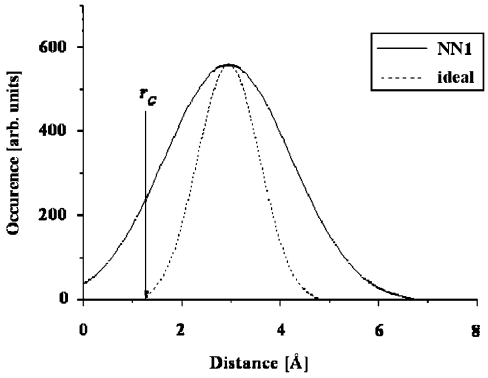


Fig. 4. Schematic illustration of the experimental next neighbour's distribution broadening and an ideal distribution for the first next neighbour.

Table 2
Summary of the average distances of the first 10 next neighbour atoms for different correlations, calculated by processing the NNE algorithm to TAP data

| Next neighbour distances in (Å) | Pd–Pd | Cu–Cu | Pd–Cu | Cu–P | P–P | Pd–P |
|---|---|---|---|---|---|---|
| NN1 | 2.21 | 3.01 | 3.08 | 3.15 | 3.16 | 3.19 |
| NN2 | 3.02 | 4.09 | 4.13 | 4.26 | 4.25 | 4.27 |
| NN3 | 3.56 | 4.80 | 4.85 | 4.99 | 5.00 | 5.02 |
| NN4 | 3.98 | 5.37 | 5.41 | 5.58 | 5.58 | 5.60 |
| NN5 | 4.33 | 5.85 | 5.88 | 6.08 | 6.08 | 6.08 |
| NN6 | 4.63 | 6.27 | 6.29 | 6.50 | 6.50 | 6.51 |
| NN7 | 4.91 | 6.64 | 6.66 | 6.89 | 6.89 | 6.89 |
| NN8 | 5.16 | 6.98 | 6.99 | 7.23 | 7.24 | 7.24 |
| NN9 | 5.39 | 7.30 | 7.30 | 7.55 | 7.56 | 7.56 |
| NN10 | 5.59 | 7.58 | 7.59 | 7.84 | 7.86 | 7.86 |

The distances are in Å.

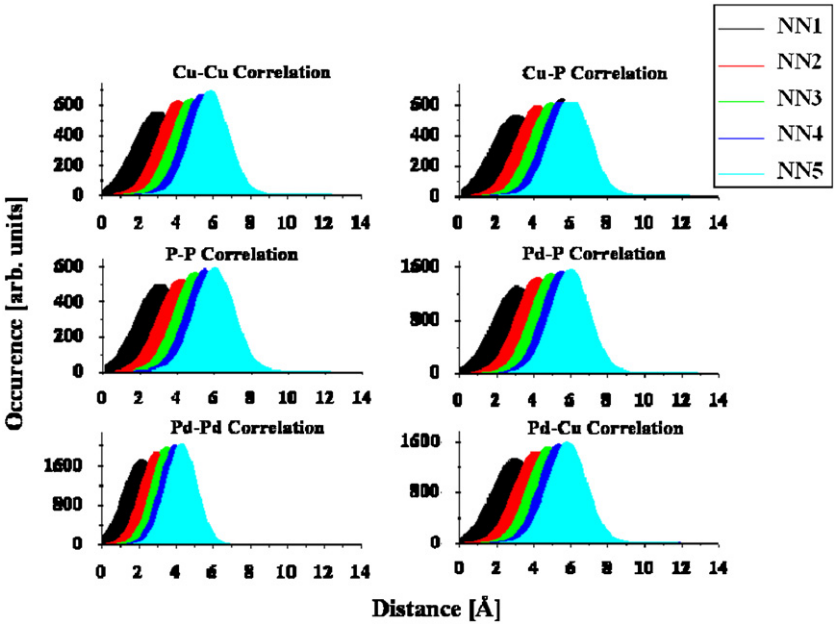


Fig. 5. The distance distribution of first five next neighbours for all correlations after Gaussian fit. The distances assigned as NN*i* shows the distance distribution of *i*th next neighbouring atom for the respective correlation. Each graph presents the probability of finding the first five next neighbours of the respective correlation.

lead to smaller values of FWHM. The distances of maximum occurrence of each distribution give the maximum probability of finding a respective atom at those distances. The results for all correlations are summarized in Table 2.

## 5. Comparison with RDF

The best explanation for these results is to make a comparison with well-established radial distributions known from different diffraction techniques. Fig. 6 illustrates a typical radial distribution function for amorphous alloys showing first and second coordination shells. However, in the case of NNE instead of cumulative shell, exact distances of each next neighbour contributing to respective coordination shell can be described. As discussed earlier, RDF provides information about average number of atoms at certain distances, hence, NN1, NN2 and/or NN3 might contribute to the first coordination shell and the remaining ones (NN4, NN5, etc.,) can be a part of next coordination shell, as will be discussed further in comparison with the diffraction results.

## 6. Discussion

### 6.1. Comparison with the diffraction results

Table 2 illustrates the NN distances for the first 10 atoms of all correlations for the investigated material. The order of finding atoms next to each other is the same as presented in this table, i.e., Pd–Pd, Cu–Cu, Pd–Cu, Cu–P, P–P and Pd–P. The first neighbour for P–P is found at a distance of 3.16 Å as compared to the expected distance of 2.12 Å (covalent diameter of P), which means that they are rarely neighbours to each other as reported earlier [17,18]. Since, the partial RDFs of the material analysed from scattering techniques are not yet reported, a comparison is made with already available data in the literature. Albeit, the referred experiments were done mostly on binary alloys except (Pd–Ni–P), it provides somewhat analogous information for a comparison. The Pd–Pd correlation reported by Duine et al. [19] is reproduced in Fig. 7. The arrows pointing towards the abscissa show the next neighbour atomic positions deduced from the present work. NN1 and NN2 appear to contribute to the first coordination shell while, NN3–NN10 are contributing to the second coordinate shell. Taking the average of the corresponding neighbouring distances i.e., for NN1 and NN2 for the first shell gives a distance of 2.6 Å while other neighbours contributing to the second coordinate shell, i.e. average of NN3–NN10 gives an average distance of 4.7 Å, these values are in a very good agreement with the corresponding peaks in Pd–Pd partial RDF. A similar comparison is shown in Fig. 8 for Cu–Cu [20] and in Fig. 9 for P–P correlation [21].

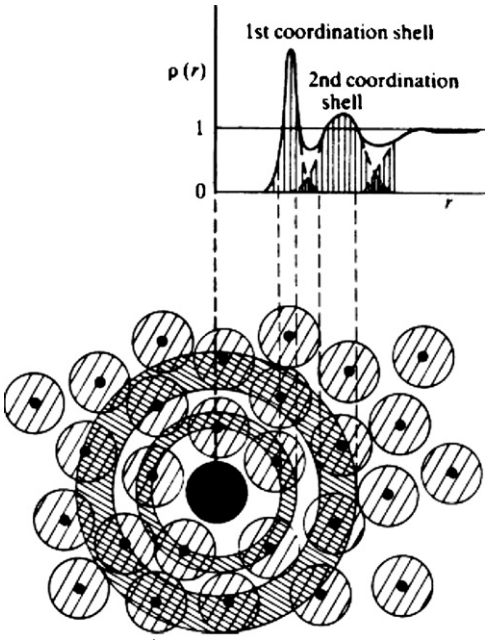


Fig. 6. Schematic illustration of the structural origin of certain features in the density function $\rho(r)$ for an amorphous solid [16].

### 6.2. Dependence of evaluation data on evaporation field at tip surface ($F_o$) and geometrical field factor ($K_f$)

A comparison of the next neighbouring atomic distances calculated by processing the NNE algorithm on atomic reconstructions for different $F_oK_f$ factors [22] is given in

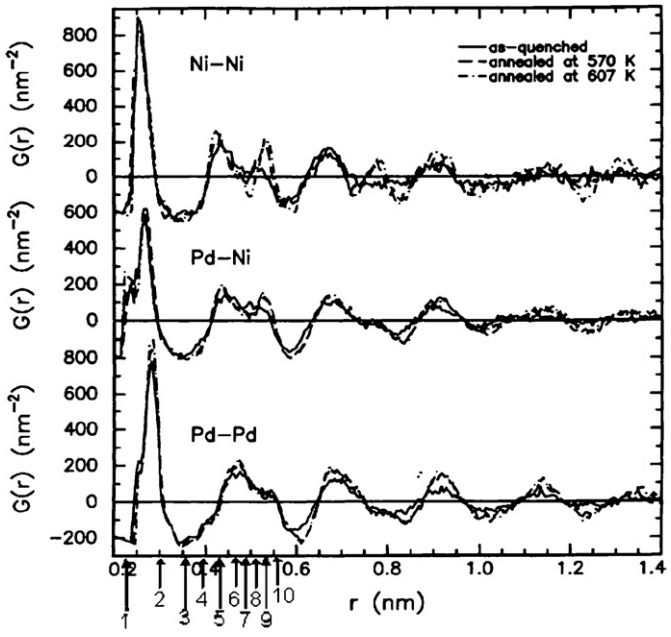


Fig. 7. Reduced partial RDF of amorphous $Pd_{52}Ni_{32}P_{16}$ alloy for the as quenched and annealed states calculated by Duine et al. [19]. The arrows indicated along the abscissa are the distances of first 10 next neighbours for Pd–Pd correlation, calculated by processing the NNE algorithm in the present work.

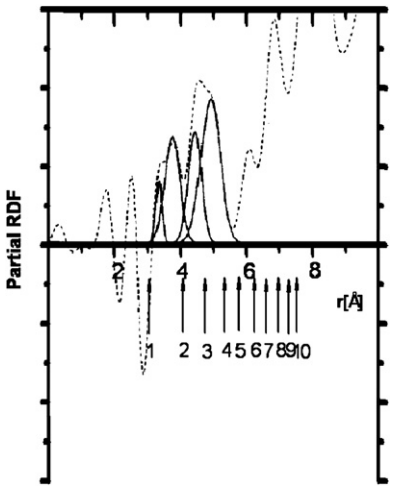


Fig. 8. Reduced partial RDF of $Cu_{33}Y_{67}$ glass and Gaussian components of the nearest neighbour region, characterized by Maret et al. [20]. The arrows indicated along the abscissa are the distances of first 10 next neighbours for Cu–Cu correlation, calculated by processing the NNE algorithm in the present work.

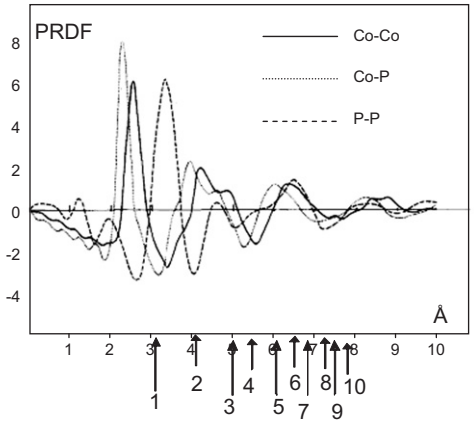


Fig. 9. Reduced partial RDF of $Co_{80}P_{20}$ amorphous alloy characterized by Sadoc et al. [21]. The arrows indicated along the abscissa are the distances of first 10 next neighbours for P–P correlation, calculated by processing the NNE algorithm in the present work.

Table 3. The estimated $F_oK_f$ value used for this alloy system is 24 V/Å. The next neighbouring distances are almost unaffected for smaller deviations in the estimated value of $F_oK_f$. However, there are pronounced differences for larger ($>\pm5$ V/Å) $F_oK_f$ variations especially for the smaller values of $F_oK_f$ (e.g., for the distance distribution of Pd–Pd and P–P). A lower $F_oK_f$ value than the estimated one results in larger next neighbour atomic distances and vice versa.

A comparison of the next neighbouring atomic distances calculated by processing the NNE algorithm on atomic reconstructions for different average atomic volumes ($\Omega_{av}$) [22] manifests the strong dependence of the next neighbouring atomic distances on the $\Omega_{av}$ values (not presented here). A slight increase in the average atomic volume results in a remarkable increase in the next neighbour distances and vice versa. Hence, wrong $\Omega_{av}$ and $F_oK_f$ parameters can result in a small shift of all distributions to higher or lower distances. The variation of the NNs with respect to different values of $\Omega_{av}$ and $F_oK_f$ also reflect the dependence on both depth and lateral resolution. These parameters affect differently both depth and lateral scaling, hence, resulting in different average NNs. These results corroborate the influence of the reconstruction parameters as reported in detail elsewhere [23,24].

Table 3
Comparison of the average distances of the first five next neighbour atoms for different correlations, calculated for different $F_oK_f$ values

| | Pd–Pd | | | | | Cu–Cu | | |
|---|---|---|---|---|---|---|---|---|
| $F_oK_f$ (V/Å) | 30 | 25 | 24 | 23 | 15 | 25 | 24 | 23 |
| NN1 | 2.20 | 2.20 | 2.21 | 2.23 | 2.27 | 3.01 | 3.01 | 3.03 |
| NN2 | 3.02 | 3.01 | 3.02 | 3.05 | 3.07 | 4.07 | 4.09 | 4.11 |
| NN3 | 3.55 | 3.54 | 3.56 | 3.59 | 3.60 | 4.79 | 4.80 | 4.82 |
| NN4 | 3.99 | 3.96 | 3.98 | 4.01 | 4.02 | 5.36 | 5.37 | 5.38 |
| NN5 | 4.35 | 4.31 | 4.33 | 4.36 | 4.37 | 5.84 | 5.85 | 5.86 |

| | Cu–P | | | Pd–P | | | Pd–Cu | | |
|---|---|---|---|---|---|---|---|---|---|
| | 25 | 24 | 23 | 25 | 24 | 23 | 25 | 24 | 23 |
| NN1 | 3.12 | 3.15 | 3.19 | 3.12 | 3.19 | 3.22 | 3.03 | 3.08 | 3.12 |
| NN2 | 4.18 | 4.26 | 4.30 | 4.20 | 4.27 | 4.32 | 4.09 | 4.13 | 4.16 |
| NN3 | 4.93 | 4.99 | 5.03 | 4.92 | 5.02 | 5.07 | 4.80 | 4.85 | 4.87 |
| NN4 | 5.51 | 5.58 | 5.61 | 5.49 | 5.60 | 5.65 | 5.36 | 5.41 | 5.43 |
| NN5 | 5.99 | 6.08 | 6.10 | 5.97 | 6.08 | 6.13 | 5.83 | 5.88 | 5.90 |

| | P–P | | | | |
|---|---|---|---|---|---|
| | 30 | 25 | 24 | 23 | 15 |
| NN1 | 3.15 | 3.10 | 3.16 | 3.25 | 3.22 |
| NN2 | 4.25 | 4.19 | 4.25 | 4.31 | 4.32 |
| NN3 | 4.99 | 4.93 | 5.00 | 5.05 | 5.07 |
| NN4 | 5.59 | 5.51 | 5.58 | 5.63 | 5.64 |
| NN5 | 6.11 | 6.00 | 6.08 | 6.12 | 6.13 |

The distances are in Å.

### 6.3. Structural features down to next neighbouring atoms

In order to find out any correlation among the distances of different neighbours, a normalization should be made by a certain factor, e.g. normalizing with the diameter of respective atoms. The distance of the respective first neighbour NN*i* is used for normalizing, firstly because it contains the average diameter of both atoms and secondly because of the difficulties in accessing the exact diameter of the atoms in amorphous states. The normalized distances are summarized in Table 4. Surprisingly, the resultant ratios after normalization are similar for all elemental correlations, showing that there is a steric relationship rather than chemical. A steric dependence can also be

Table 4
The ratio for different elemental correlations after normalizing the average distances of the first 10 next neighbours by the average distance of first neighbouring atom

| | Pd–Pd | Cu–Cu | Pd–Cu | Cu–P | P–P | Pd–P | Average ratio |
|---|---|---|---|---|---|---|---|
| NN2/NN1 | 1.36 | 1.36 | 1.34 | 1.35 | 1.34 | 1.34 | 1.35 |
| NN3/NN1 | 1.61 | 1.60 | 1.57 | 1.59 | 1.58 | 1.57 | 1.59 |
| NN4/NN1 | 1.80 | 1.79 | 1.75 | 1.77 | 1.77 | 1.76 | 1.77 |
| NN5/NN1 | 1.96 | 1.95 | 1.91 | 1.93 | 1.92 | 1.91 | 1.93 |
| NN6/NN1 | 2.10 | 2.09 | 2.04 | 2.07 | 2.06 | 2.04 | 2.06 |
| NN7/NN1 | 2.22 | 2.21 | 2.16 | 2.19 | 2.18 | 2.16 | 2.19 |
| NN8/NN1 | 2.33 | 2.32 | 2.27 | 2.30 | 2.29 | 2.27 | 2.30 |
| NN9/NN1 | 2.44 | 2.43 | 2.37 | 2.40 | 2.39 | 2.37 | 2.40 |
| NN10/NN1 | 2.53 | 2.52 | 2.46 | 2.49 | 2.49 | 2.47 | 2.49 |

The distances are in Å.

inferred from the RDFs. In the case of the RDFs, the neighbouring coordination shells follow a certain periodicity. On the other hand, our finding shows that even neighbouring atoms are arranged at certain definite order. Häussler suggests that the repetition of the coordination shells is based on the Friedel oscillation [25]. However, Teichler found such a relation in RDFs calculated from the pair potential simulations, justified purely by steric considerations [26]. Nevertheless, for both cases, the coordination shells follow a certain periodicity. The findings from the present results, however, reveal such an atomic ordering/periodicity even exists down to those next neighbouring atoms that are responsible for the coordination shells in RDFs.

## 7. Conclusion

A novel algorithm is enunciated to elucidate the NN atomic vicinity from the data, analysed using TAP. In the present work, a Pd based bulk amorphous alloy is characterized by using this algorithm. First 10 next neighbours for all elemental correlations were evaluated alone from the TAP data, which for multi-component systems is difficult, otherwise. A comparison of the FWHM among different elemental correlations in Fig. 5 reveals the following trend, FWHM for Pd–Pd < Cu–Cu < P–P due to the compositional dependence (a higher concentration leads to a smaller FWHM). The distribution of next neighbouring atomic distances shows that for this system, the Pd–Pd atoms have the highest probability to be the next neighbours to each other. The fact that P is not a direct next neighbour to another P atom is also obvious from these results. The distances for the first 10 next neighbours of different elemental correlations are in good agreement with the data available in the literature. The findings from the present work enables for the first time to envisage the atoms responsible for the coordination peaks in RDFs. Normalizing the distances by the first next neighbour distance NN1 yields a ratio similar for all elemental correlations showing that their exist a certain order among the atoms, irrespective of the chemical nature of the atoms. Such an atomic ordering is already known for the coordination peaks in RDFs [25,26]. The algorithm utilized in the present work allows specifying atom positions and chemical identities of the next neighbouring atoms for amorphous materials in real space which are difficult to access alone from RDFs. This method may also help in selecting the best reconstruction parameters, and to quantify the possible errors on NN's distances. Moreover, substantial information can be extracted on short-range ordering in amorphous alloys by comparing the NNs in different heat-treated states.

## Acknowledgements

The authors would like to thank Prof. Dr. H. Teichler and Dr. M. Guerdane of the Institut für Materialphysik, Göttingen, Germany and F. Danoix of GPM, UMR 6634 CNRS, Rouen university, Rouen, France for many valuable discussions and critical comments on the manuscript and Dr. D. J. Safarik of Los Alamos National Laboratory, MST Division, Los Alamos, USA to kindly provide the samples. The Lower Saxony's German government is gratefully acknowledged for the financial support of the project.

## References

[1] R.C. O'Handley, J. Appl. Phys. 62-10 (1987) R15.
[2] J. Dixmier, J.F. Sadoc, in: Metallic Glasses; Materials Science Seminar, American Society for Metals, Metals Park, OH, 1976, p. 97.
[3] M. Oehring, P. Hassen, J. Phys. 47 (C7) (1986) 275.
[4] M.P. Macht, N. Wanderka, A. Wiedenmann, H. Wollenberger, Q. Wei, H.J. Fecht, S.G. Klose, Mater. Sci. Forum 65 (1996) 225.
[5] M.K. Miller, Mater. Sci. Eng. A 250 (1998) 133.
[6] R. Busch, S. Schneider, A. Peker, W.L. Johnson, Appl. Phys. Lett. 67 (1995) 1544.
[7] A. Heinrich, T. Al-kassab, R. Kirchheim, in: Conference Proceedings IFES04 (2004) 134.
[8] F. De Geuser, W. Lefebvre, D. Blavette, Phil. Magz. Lett. 86-4 (2006) 227.
[9] C.K. Sudbrack, Ph.D. Thesis, Northwestern University, 2004.
[10] A. Shariq, T. Al-Kassab, in: Conference Proceedings of the SCANDEM 2006 (2006), 40.
[11] D.J. Larson, D.T. Foord, A.K. Petford-Long, T.C. Anthony, I.M. Rozdilsky, A. Cerezo, G.D.W. Smith, Ultramicroscopy 75 (1998) 147.
[12] D. Blavette, B. Deconihout, A. Bostel, J.M. Sarrau, M. Bouet, A. Menand, Rev. Sci. Instrum. 64-10 (1993) 2911.
[13] T. Al-Kassab, H. Wollenberger, G. Schmitz, R. Kirchheim, in: F. Ernst, M. Rühler (Eds.), High Resolution Imaging and Spectrometry of Materials, Springer Series of Material Science, Springer, Berlin, Heidelberg, 2003, pp. 274–320 (Chapter 6).
[14] M.K. Miller, T.D. Shen, R.B. Schwarz, J. Non-cryst. Solids 317 (2003) 10.
[15] A. Shariq, PhD Thesis, Göttingen University, 2006.
[16] S.R. Elliott, Physics of amorphous materials, second edition, Longman Group, UK limited, 1990.
[17] J. Wong, in: H.-J. Güntherodt, H. Beck (Eds.), EXAF studies of metallic glasses, Glassy Metals I; Ionic Structure, Electronic Transport and Crystallization, Topics in Applied Physics, Vol. 46, Springer BHNYT, Berlin, 1981, pp. 45–78 (Chapter 4).

[18] P.H. Gaskell, in: H. Beck, H.-J. Güntherodt (Eds.), Glassy Metals II; Atomic Structure and Dynamics, Electronic Structure and Magnetic Properties, Topics in Applied Physics, Vol. 53, Springer BHNYT, Berlin, 1983, pp. 5–50.
[19] P.A. Duine, J. Sietsma, B.J. Thijsse, Phys. Rev. B 50-18 (1994) 13240.
[20] M. Maret, P. Chieux, P. Hicter, M. Atzmon, W.L. Johnson, J. Phys. F: Met. Phys. 17 (1987) 315.
[21] J.F. Sadoc, J. Dixmier, Mater. Sci. Eng. 23 (1976) 187.
[22] M.K. Miller, G.D.W. Smith, Atom Probe Microanalysis; Principles and Applications to Materials Problems, Materials Research Society, 1989.
[23] P. Bas, A. Bostel, B. Deconihout, D. Blavette, Appl. Surf. Sci. 87/88 (1995) 298.
[24] F. Vurpillot, L. Renaud, D. Blavette, Ultramicroscopy 95 (2003) 223.
[25] P. Häussler, J. Physique (Paris) C 8 (1985) 361.
[26] H. Teichler, Unpublished data, Private communication, Institut für Materialphsik, Universität Göttingen, 2006.